Advances in Applied Mathematics and Mechanics
Adv. Appl. Math. Mech., Vol. **17**, No. 1, pp. 350-372

DOI: 10.4208/aamm.OA-2022-0166
February 2025

# A Boundary Mapped Collocation Method for the Analysis of the Arbitrarily Shaped Plates

Zhentian Huang[1,2,3,*], Dong Lei[3], Zi Han[4], Heping Xie[2] and Jianbo Zhu[2]

[1] *School of Civil Engineering & Architecture, East China Jiaotong University, Nanchang, Jiangxi 330013, China*
[2] *Guangdong Provincial Key Laboratory of Deep Earth Sciences and Geothermal Energy Exploitation and Utilization, Institute of Deep Earth Sciences and Green Energy, College of Civil and Transportation Engineering, Shenzhen University, Shenzhen, Guangdong 518060, China*
[3] *College of Mechanics and Materials, Hohai University, Nanjing, Jiangsu 211100, China*
[4] *College of Civil Engineering and Architecture, Nanchang Hangkong University, Nanchang, Jiangxi 330063, China*

Received 19 June 2022; Accepted (in revised version) 1 June 2023

**Abstract.** An innovative meshless method is proposed in this paper for the bending problem of arbitrary Kirchhoff plates subjected to external force with various shapes and different boundary conditions. Without using a numerical integral, the deflection of the thin plate is approximated by using the boundary mapped collocation approach. Moreover, the computational domain discretization is just dependent on discretized nodes on the axis, while tensor product nodes have been mapped in the domain automatically. Hence, in the boundary mapped collocation implementation, the approximation functions are derived by employing the one-dimensional moving least squares technique for two-dimensional and higher-dimensional problems. Further, the virtual boundary technique is introduced to enforce the boundary conditions in the proposed method. Additionally, four numerical experiments are presented to illustrate the excellent convergence and high precision of the proposed approach.

**AMS subject classifications**: 35-04, 65N35, 68-04

**Key words**: Boundary mapped collocation method, moving least squares, Kirchhoff plate, meshless method.

*Corresponding author.
*Emails:* zhentian_huang@163.com (Z. Huang)

 

# 1 Introduction

Exploring the constructional mechanical behavior via solving various partial differential equations for engineering problems has always been one of the most challenging tasks for engineers and scientists [1]. However, it is difficult to derive analytic solutions for complex partial differential equations (PDEs). Hence, several numerical algorithms [2–4] have been proposed for solving the various PDEs [5–7]. Among these are the grid-based methods, such as the finite element method (FEM), the finite difference method (FDM), and the boundary element method (BEM) are widely used methods of numerical simulation to practice engineering. In Kirchhoff plate bending theory, flexural functions satisfy the fourth-order PDE of the plate. Since the high-order properties of the governing equation, the grid-based approaches all have faced numerous challenges e.g., the computational cost of the FEM method is high for solving high dimensional problems, the fictitious boundary technique is introduced to eliminate singularity of fundamental solutions in method of fundamental solution [8, 9]. Also, the fourth-order singularity of the kernel functions requires a complicated boundary integration technique by employing the traditional BEM. Therefore, it is of great academic interest to develop a computationally efficient and accurate numerical approach.

Remarkably, as a new numerical technique that obtains approximate solutions for PDEs by getting rid of mesh dependence, meshless approaches have recently received increasing attention in the fields of computational mechanics and computational mathematics. Since the beneficial properties such as simplifying pre-processing, high precision, and the possibility of solving partial equations without resorting to any background grids in the computation domain, meshless approaches have become an effective alternative to the conventional grid-based technique [10].

In this regard, some meshless methods have been directly adopted for solving numerous practical engineering problems [11, 12], the diffuse element method (DEM) [13], the element-free Galerkin (EFG) method [14], the reproducing kernel particle method (RKPM) [15], the h-p clouds methods [16], the meshless local Petrov-Galerkin (MLPG) method [17], the finite point method (FPM) [18], the local Petrov-Galerkin approach with moving Kriging interpolation [19–21], the element-free kp-Rize method [22], the meshless with boundary integral equation methods [23–25], the interpolating element-free Galerkin method [26], the complex variable meshless method [27], the Burton–Millertype-type singular boundary method [28], the localized Chebyshev collocation method [29], the localized method of fundamental solutions [30] and the boundary collocation method [31]. In this regard, meshless techniques are particularly adapted for the analysis of the plate and shell structure bending problems. Krysl and Belytschko in [32, 33] approximated the deflection by employing the EFGM. Sadamoto and Tanaka et al. in [34] introduced the RKPM for studying plate and membrane problems. Leitão in [35] proposed radial basis functions (RBFs) to analyze the Kirchhoff plate problems. Sadamoto and Ozdemir et al. in [35] solved buckling problems for cylindrical shells employing the reproducing kernel (RK) meshfree method. Long and Atluri in [36] introduced the MLPG

approach for solving plate bending problems. Battaglia and Matteo in [37] developed the line element-less method (LEM) for arbitrarily shaped thin plates and so on.

In this context, a meshless method of the boundary mapped collocation (BMC) method will be developed for solving the Kirchhoff plate problems. As has been illustrated in Huang and Lei for the analysis of wave propagation [38, 39], two-dimensional elastic dynamics [40, 41], and three-dimensional elastic static problems [42], the BMC approach is a real meshless technique due to no boundary or domain grids in the discretization procedure. Moreover, since this method requires no integrals in the formulation, its computational cost is substantially lower than the weak-form meshless methods. Further, the BMC method has the Kronecker delta property in not only the shape functions but also their derivatives since the substitution technique is introduced to enforce the various boundary conditions. Additionally, this paper is concluded with a section on numerical experiments. The square, triangular, elliptical, and irregular plates are analyzed to verify the precision and computational efficiency of the BMC approach, getting rid of the grids and integrals, with different boundary and external force conditions. Moreover, the dependence of the accuracy and convergence of the presented method on the choice for the various basis and weight functions is investigated.

## 2 Kirchhoff plate bending problem definition

The governing equation for the Kirchhoff plate is presented according to the classical thin plate bending theory. Considering a Kirchhoff plate of the flexural rigidity $D$ with boundary $\Gamma$ and domain $\Omega$, under a transversal load $q$, known as Kirchhoff plate, as shown in Fig. 1. The governing differential equation for the deflection $w(x,y)$ is the fourth-order PDEs which can be written as

$$\nabla^4 w = \frac{q}{D}, \tag{2.1}$$

where $w$ is the transversal deflection,

$$\nabla^4 \equiv \nabla^2 \cdot \nabla^2 = \frac{\partial^4}{\partial x^4} + 2\frac{\partial^4}{\partial x^2 \partial y^2} + \frac{\partial^4}{\partial y^4}, \quad D = \frac{Eh^3}{12(1-\mu^2)}$$

is the flexural stiffness, $E$ is modulus of elasticity, $h$ is uniform thickness, and $\mu$ is the Poisson's ratio.

According to the Kirchhoff plate bending theory, the moments $M_x$, $M_y$, $M_{xy}$ can be expressed as follows

$$M_x = -D\left(\frac{\partial^2 w}{\partial x^2} + \mu\frac{\partial^2 w}{\partial y^2}\right), \tag{2.2a}$$

$$M_y = -D\left(\frac{\partial^2 w}{\partial y^2} + \mu\frac{\partial^2 w}{\partial x^2}\right), \tag{2.2b}$$

$$M_{xy} = -D(1-\mu)\frac{\partial^2 w}{\partial x \partial y}. \tag{2.2c}$$

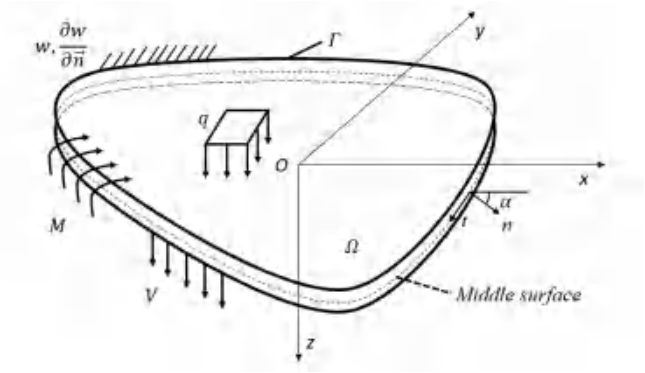


Figure 1: Kirchhoff plate with arbitrary shape.

The shearing forces $V_x$ and $V_y$ are given by

$$V_x=-D\frac{\partial}{\partial x}\left(\frac{\partial^2 w}{\partial x^2}+\frac{\partial^2 w}{\partial y^2}\right), \tag{2.3a}$$

$$V_y=-D\frac{\partial}{\partial y}\left(\frac{\partial^2 w}{\partial x^2}+\frac{\partial^2 w}{\partial y^2}\right). \tag{2.3b}$$

In addition, the boundary conditions can be defined as

**Free edge**

$$M_n=0,\quad V_n=0,$$

where the normal effective shear $V_n$ applied at the edged is written as

$$V_n=-D\left\{n_x\frac{\partial}{\partial x}\nabla^2 w+n_y\frac{\partial}{\partial y}\nabla^2 w+(1-\mu)\left(n_x\frac{\partial}{\partial y}-n_y\frac{\partial}{\partial x}\right)\left[\left(n_x^2-n_y^2\right)\frac{\partial^2 w}{\partial x\partial y}+n_x n_y\left(\frac{\partial^2 w}{\partial y^2}-\frac{\partial^2 w}{\partial x^2}\right)\right]\right\}. \tag{2.4}$$

**Simply supported edge**

$$w=0,\quad M_n=0, \tag{2.5}$$

where the normal bending moment $M_n$ can be expressed as

$$M_n=-D\left[\mu\nabla^2 w+(1-\mu)\left(n_x^2\frac{\partial^2 w}{\partial x^2}+n_y^2\frac{\partial^2 w}{\partial y^2}+2n_x n_y\frac{\partial^2 w}{\partial x\partial y}\right)\right]. \tag{2.6}$$

**Clamped edge**

$$w=0,\quad n_x\frac{\partial w}{\partial n_x}+n_y\frac{\partial w}{\partial n_y}=0. \tag{2.7}$$

# 3 BMC method for Kirchhoff plate bending problems

## 3.1 Moving least squares approximation

A brief introduction to the moving least squares (MLS) technique, as the basics of the BMC approach is given in this section. Considering the computational domain $\Omega$ for an unknown function $u(x)$, which is approximated by a polynomial expansion within a small support domain $\Omega_0$ of numerous random discrete nodes. The approximation equations are defined as follows

$$u(x) \cong \hat{u}(x) = \sum_{i=1}^{k} p_i(x)\alpha_i = \mathbf{p}(x)^T \boldsymbol{\alpha}(x) = \mathbf{N}\mathbf{u}, \tag{3.1}$$

where coefficients $\boldsymbol{\alpha}(x) = [\alpha_1, \alpha_2, \cdots, \alpha_k]^T$, and vector $\mathbf{p}(x)$ is a complete monomial basis of order $k$ containing typically monomials within the two/three-dimensional space coordinates. The linear base polynomials $\mathbf{p}^T(x) = [1, x]$, $(k=2)$, and the quadratic base polynomials $\mathbf{p}^T(x) = [1, x, x^2]$, $(k=3)$ are adopted for onedimensional space. The approximation equations can be written as follows in matrix

$$\mathbf{u}^h = \begin{bmatrix} u_1^h \\ u_2^h \\ \vdots \\ u_m^h \end{bmatrix} \cong \begin{bmatrix} \hat{u}_1^h \\ \hat{u}_2^h \\ \vdots \\ \hat{u}_m^h \end{bmatrix} = \begin{bmatrix} \mathbf{p_1^T} \\ \mathbf{p_2^T} \\ \vdots \\ \mathbf{p_m^T} \end{bmatrix} \boldsymbol{\alpha} = \mathbf{C}\boldsymbol{\alpha}, \tag{3.2}$$

where $\mathbf{u}^h$ are the approximation values at the discrete nodes.

The coefficient $\boldsymbol{\alpha}(x)$ is obtained by calculating the minimum for a weighted discrete $L_2$ norm, which is given as follow

$$J = \sum_{j=1}^{m} \omega_j(x) \left( u_j^h - \hat{u}_j^h \right)^2, \tag{3.3}$$

where $\omega_j(x)$ is the weight function of support domain at the discrete node $x_j$ with $\omega(x) > 0$. In this regard, the exponential function, the Gaussian function and the cone function, are introduced as weight function for numerical experiments within the BMC implementation, which is defined as follows

$$\omega(r) = \begin{cases} \dfrac{\exp\left(-r^2\beta^2\right) - \exp\left(-\beta^2\right)}{1 - \exp\left(-\beta^2\right)}, & r \le 1, \\ 0, & r > 1, \end{cases} \tag{3.4a}$$

$$\omega(r) = \begin{cases} \exp\left(-r^2\beta^2\right), & r \le 1, \\ 0, & r > 1, \end{cases} \tag{3.4b}$$

$$\omega(r) = \begin{cases} \left(1 - r^2\right)^n, & r \le 1, \quad n \ge 2, \\ 0, & r > 1, \end{cases} \tag{3.4c}$$

where $r=|x-x_i|/d_m$ is the threshold value of weight function, $d_m=c\times dx$ is the compact domain radius of the discrete node $x_i$, $c$ is the scale parameter of the support domain $\Omega_0$, and $dx$ is the distance between two adjacent discrete nodes.

As regards to the unknown coefficients $\boldsymbol{\alpha}(x)$, it could be deduced as follows

$$\frac{\partial J}{\partial \boldsymbol{\alpha}}=0. \tag{3.5}$$

And

$$\boldsymbol{\alpha}=\mathbf{C}^{-1}\mathbf{u}^h \quad \text{with} \quad \mathbf{C}^{-1}=\mathbf{A}^{-1}\mathbf{B}, \tag{3.6}$$

where

$$\mathbf{A}(x)=\sum_{j=1}^{m}\omega_j(x)\mathbf{p}\left(x_j\right)\mathbf{p}^{\mathrm{T}}\left(x_j\right), \tag{3.7a}$$

$$\mathbf{B}(x)=[\omega_1(x)\mathbf{p}(x_1),\omega_2(x)\mathbf{p}(x_2),\cdots,\omega_m(x)\mathbf{p}(x_m)]. \tag{3.7b}$$

Finally, the shape function of the one-dimensional MLS approach is defined by,

$$\mathbf{N}(x)=\mathbf{p}^T(x)\mathbf{C}^{-1}=\mathbf{p}^T(x)\mathbf{A}^{-1}(x)\mathbf{B}(x). \tag{3.8}$$

Also, the derivative of shape function is presented as

$$\frac{dN}{dx}=\mathbf{A}^{-1}\frac{dp}{dx}\mathbf{B}, \tag{3.9a}$$

$$\frac{d^2N}{dx^2}=\mathbf{A}^{-1}\frac{d^2p}{dx^2}\mathbf{B}. \tag{3.9b}$$

### 3.2 BMC shape function

In this section, the BMC theory is given within two-dimensional space. Considering that the two-dimensional space $\Omega$ is discretized by a dot matrix $m_1\times m_2$, and $m_1$, $m_2$ are the discrete node numbers in $x$,$y$-axis, respectively. In this regard, the BMC approximation $w^h(x,y)$ of the function $w(x,y)$ over every computational node is expressed as follows

$$w^h(x,y)=\sum_{i=1}^{m_1}\sum_{j=1}^{m_2}\mathbf{N}_i(x)\mathbf{N}_j(y)w_{ij}. \tag{3.10}$$

Here, two decoupled one-dimensional boundary shape functions $\mathbf{N}(x)$, $\mathbf{N}(y)$ concerning $x$,$y$-axis are in the same form as denoted in Eq. (3.8);

$$\mathrm{N}(x)=\mathbf{p}^T(x)\mathbf{A}^{-1}(x)\mathbf{B}(x), \tag{3.11a}$$

$$\mathrm{N}(y)=\mathbf{p}^T(y)\mathbf{A}^{-1}(y)\mathbf{B}(y), \tag{3.11b}$$

Table 1: The comparison of basis function between MLS and BMC for 2D problems.

| The order of the basis function | MLS | BMC |
|---|---|---|
| Linear | $1, x, y$ | $1, x$<br>$1, y$ |
| Quadratic | $1, x, y, xy, x^2, y^2$ | $1, x, x^2$<br>$1, y, y^2$ |
| Cubic | $1, x, y, xy, x^2, y^2, xy^2, x^2y, x^3, y^3$ | $1, x, x^2, x^3$<br>$1, y, y^2, y^3$ |

and

$$\mathbf{A}(x)=\sum_{j=1}^{m}\omega_j(x)\mathbf{p}\left(x_j\right)\mathbf{p}^{\mathrm{T}}\left(x_j\right), \tag{3.12a}$$

$$\mathbf{B}(x)=[\omega_1(x)\mathbf{p}(x_1),\omega_2(x)\mathbf{p}(x_2),\cdots,\omega_m(x)\mathbf{p}(x_m)], \tag{3.12b}$$

$$\mathbf{A}(y)=\sum_{j=1}^{m}\omega_j(y)\mathbf{p}\left(y_j\right)\mathbf{p}^{\mathrm{T}}\left(y_j\right), \tag{3.12c}$$

$$\mathbf{B}(y)=[\omega_1(y)\mathbf{p}(y_1),\omega_2(y)\mathbf{p}(y_2),\cdots,\omega_m(y)\mathbf{p}(y_m)]. \tag{3.12d}$$

Hence, the partial derivative of $\boldsymbol{w}^h$ is obtained in the form

$$\frac{\partial^{\zeta+\eta}w}{\partial^{\zeta}x\partial^{\eta}y}=\sum_{i=1}^{m_1}\sum_{j=1}^{m_2}\mathbf{N}_i^{\zeta}(x)\mathbf{N}_j^{\eta}(y)w_{ij}. \tag{3.13}$$

Additionally, the one-dimensional boundary shape functions are formally equal to the one-dimensional MLS approximation. However, the two-dimensional BMC approximation function is derived by using two one-dimensional boundary shape functions. Hence, only the one-dimensional basis functions and the one-dimensional weight function are introduced to solve two-dimensional space problems within the BMC implementation. The differences between BMC and MLS are illustrated in Table 1, Fig. 2, respectively. Table 1 shows there are no coupling terms $xy$, $xy^2$, and $x^2y$ in the BMC approach, compared with MLS method. This advantage greatly simplifies the derivation process of the shape function within two-dimensional BMC implementation. Also, Fig. 2 displays the node distribution of the MLS and BMC methods, respectively. The discrete nodes on the axis are mapped to the computational domain while the regular tensor product nodes are generated in the domain $\Omega$ automatically.

### 3.3 The BMC discrete equation for governing equation

The moment $M$ is defined as follow:

$$M=\frac{M_x+M_y}{1+\mu}. \tag{3.14}$$

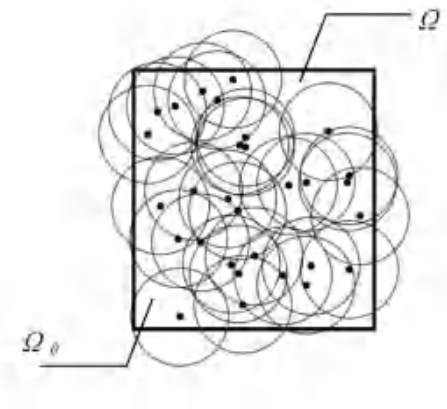


(a) Circular support of the MLS

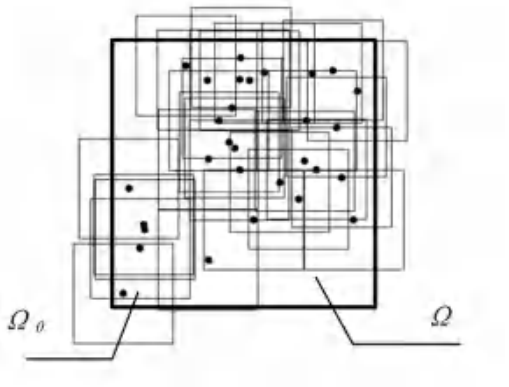


(b) Rectangle support of the MLS

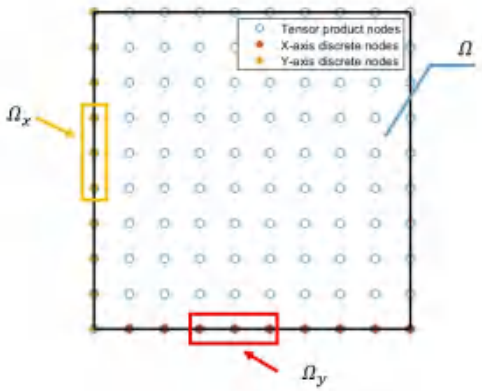


(c) The support domain of the BMC

Figure 2: The support domain of the weight function of the MLS approximation and the BMC approximation. $\Omega$ is the computational domain, $\Omega_0$ is the support domain of one discrete node. (a) Circular support domain of the MLS, (b) Rectangle support domain of the MLS, (c) The support domain of the weight function of BMC, $\Omega_x$ is the support domain of the discrete node on $x$-axis, $\Omega_y$ is the support domain of the discrete node on $y$-axis, corresponding tensor product nodes are generated automatically employing $x$-axis and $y$-axis discrete nodes.

The fourth-order governing equation could be substituted by two second-order Poisson's equations as

$$\nabla^2 M = -q, \quad \nabla^2 w = -\frac{M}{D}. \tag{3.15}$$

Hence, the high-order governing equation of the plate bending problems, i.e., Eq. (2.1), reduces to low-order Eq. (3.15) in succession. Further, according to the reduced-order

Eq. (3.15), $M$ and $w$ can be expressed employing the BMC approximation:

$$w=\sum_{i=1}^{m_1}\sum_{j=1}^{m_2}\mathbf{N}_i(x)\mathbf{N}_j(y)w_{ij}, \tag{3.16a}$$

$$M=\sum_{i=1}^{m_1}\sum_{j=1}^{m_2}\mathbf{N}_i(x)\mathbf{N}_j(y)M_{ij}. \tag{3.16b}$$

Now, substituting Eqs. (3.6) and (3.9) into (3.8), we can obtain:

$$\sum_{i=1}^{m_1}\sum_{j=1}^{m_2}\mathbf{N}_i^{(2)}(x)\mathbf{N}_j(y)M_{ij}+\sum_{i=1}^{m_1}\sum_{j=1}^{m_2}\mathbf{N}_i(x)\mathbf{N}_j^{(2)}(y)M_{ij}=-q, \tag{3.17a}$$

$$\sum_{i=1}^{m_1}\sum_{j=1}^{m_2}\mathbf{N}_i^{(2)}(x)\mathbf{N}_j(y)w_{ij}+\sum_{i=1}^{m_1}\sum_{j=1}^{m_2}\mathbf{N}_i(x)\mathbf{N}_j^{(2)}(y)w_{ij}=-\frac{M}{D}. \tag{3.17b}$$

For simplicity, the boundary shape functions $\mathbf{N}(x)$, $\mathbf{N}(y)$ are expressed as $\mathbf{N}_1$, $\mathbf{N}_2$, respectively. Similarly, the shape function derivatives for the BMC approach are written as $\mathbf{N}_1^{(1)}$, $\mathbf{N}_2^{(1)}$, $\mathbf{N}_1^{(2)}$, $\mathbf{N}_2^{(2)}$, $\mathbf{N}_1^{(3)}$, $\mathbf{N}_2^{(3)}$. Hence, the system in the matrix form can be represented as

$$\begin{bmatrix} \mathbf{N}_1^{(2)}\otimes\mathbf{I}_2+\mathbf{I}_1\otimes\mathbf{N}_2^{(2)} & \mathbf{I} \\ 0 & \mathbf{N}_1^{(2)}\otimes\mathbf{I}_2+\mathbf{I}_1\otimes\mathbf{N}_2^{(2)} \end{bmatrix}\begin{bmatrix} w \\ u \end{bmatrix}=\begin{bmatrix} 0 \\ p \end{bmatrix}, \tag{3.18}$$

where $\mathbf{I}_1$, $\mathbf{I}_2$ is the unit matrix with the size equal to the number of discrete points on $x$-axis and $y$-axis, respectively, and the symbol $\otimes$ is the Kronecker product. Further, the discretization equation is simplified as follows

$$\mathbf{KU}=\mathbf{F}. \tag{3.19}$$

Similarly, the normal bending moment $M_n$ and the effective shear $V_n$ can also be written as following

$$\begin{aligned} M_n=-D\Big[&\left(\mu+(1-\mu)n_x^2\right)\mathbf{N}_1^{(2)}\otimes\mathbf{I}_2+\left(\mu+(1-\mu)n_y^2\right)\mathbf{I}_1\otimes\mathbf{N}_2^{(2)} \\ &+2(1-\mu)n_xn_y\mathbf{N}_1^{(1)}\otimes\mathbf{N}_2^{(1)}\Big]w, \end{aligned} \tag{3.20a}$$

$$V_n=-D\left(V_1+V_2+V_3\right), \tag{3.20b}$$

where

$$\begin{aligned} V_1&=n_x\left(\mathbf{N}_1^{(3)}\otimes\mathbf{I}_2+\mathbf{N}_1^{(1)}\otimes\mathbf{N}_2^{(2)}\right)+n_y\left(\mathbf{N}_1^{(2)}\otimes\mathbf{N}_2^{(1)}+\mathbf{I}_1\otimes\mathbf{N}_2^{(3)}\right), \\ V_2&=(1-\mu)\left[n_x\left(n_x^2-n_y^2\right)\mathbf{N}_1^{(1)}\otimes\mathbf{N}_2^{(2)}+n_x^2n_y\left(\mathbf{I}_1\otimes\mathbf{N}_2^{(3)}-\mathbf{N}_1^{(2)}\otimes\mathbf{N}_2^{(1)}\right)\right], \\ V_3&=-(1-\mu)\left[n_y\left(n_x^2-n_y^2\right)\mathbf{N}_1^{(2)}\otimes\mathbf{N}_2^{(1)}+n_xn_y^2\left(\mathbf{N}_1^{(1)}\otimes\mathbf{N}_2^{(2)}-\mathbf{N}_1^{(3)}\otimes\mathbf{I}_2\right)\right]. \end{aligned}$$

Additionally, the detailed procedure of the boundary conditions (BCs) imposing is introduced in Huang and Lei et al. (2020). Notably, the symbol $\otimes$ represents the Kronecker product of matrices, which can be expressed as

$$\mathbf{H}_{(m_1\times m_2)}\otimes\mathbf{G}_{(m_3\times m_4)}\begin{bmatrix} h_{1,1}g_{1,1} & \cdots & h_{1,m_2}g_{1,m_4} \\ \vdots & \ddots & \vdots \\ h_{m_1,1}g_{m_3,1} & \cdots & h_{m_1,m_2}g_{m_3,m_4} \end{bmatrix}. \tag{3.21}$$

where $\mathbf{H}$, $\mathbf{G}$ are $m_1$ by $m_2$ and $m_3$ by $m_4$ matrix, respectively.

# 4 Numerical examples

Considering different geometric shapes, and boundary conditions, four numerical experiments are examined to validate the BMC approach. The FEM analyses are performed using COMSOL 5.6, while the BMC codes are performed using Matlab 2018b. For illustrating the convergence and estimate the error of the presented method, the relative error is defined as

$$\text{Error}_{\text{L}_2}=\frac{\left\{\sum_{i=1}^{N}[\tilde{f}(i)-f(i)]^2\right\}^{1/2}}{\left\{\sum_{i=1}^{N}[f(i)]^2\right\}^{1/2}}, \tag{4.1}$$

where $\tilde{f}$ and $f$ denote the numerical results and analytical results, respectively, $N$ is the number of computational nodes.

## 4.1 A classical benchmark test

The convergence and stability of the BMC approach for solving Kirchhoff plate problems are analyzed by calculating the node deflections. The influences of the basis function, weight function on the accuracy, and convergence rate for the presented approach are descripted in detail at length.

In the first experiment, considering a well-known benchmark that a square thin plate under an evenly distributed external force with four sides simply-supported to verify the convergence of the BMC method is displayed in Fig. 3. In addition, the condition number for stiffness matrices is used for the stability analysis of the proposed method. Also, the Navier series solution (as an exact solution) of the benchmark test is defined as

$$w=\frac{16q}{\pi^6 D}\sum_{m=1,3,\cdots}^{\infty}\sum_{n=1,3,\cdots}^{\infty}\frac{\sin\frac{m\pi x}{a}\sin\frac{n\pi y}{a}}{mn\left(\frac{m^2}{a^2}+\frac{n^2}{a^2}\right)}, \tag{4.2}$$

where $D$ is the flexural rigidity, $q$ is an evenly distributed force, and $a$ is the edge length. Assume that $q=1000\text{N}/\text{m}^2$ and $a=1.0\text{m}$. The other parameters are given as follows: elasticity modulus $E=2.1\times10^{11}\text{Pa}$, plate thickness $h=0.001\text{m}$, Poisson ratio $v=0.25$.

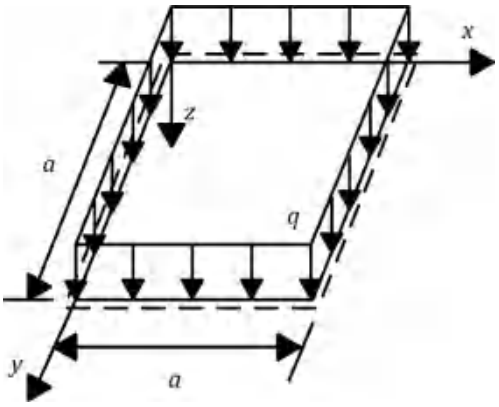


Figure 3: A square plate subjected to a uniformly distributed load with all edges simply-supported.

The uniform point distributions $11\times11$, $21\times21$, $31\times31$, $41\times41$ are employed, respectively, for analyzing the relative errors for the BMC methods with quadratic, cubic and quartic basis functions and the exponential weight function. The numerical results of relative errors and condition numbers for the stiffness matrix are shown in Figs.4 and 5, respectively. It could be observed that the smallest relative error happened on the quartic basis function results. Hence, the higher-order basis function can yield more accurate results than the lower-order basis function. Meanwhile, with the number of boundary discrete nodes increasing, the quartic and cubic basis functions give larger condition numbers than the quadratic basis function.

Employing the exponential, Gauss, and cone weight functions, and the quartic basis function, the relative errors of the BMC results are presented in Fig. 6. In this regard, using the exponential weight function could give more accurate results than the gauss and cone weight functions. In addition, the results of condition numbers for the computational matrices with different weight functions while the exponential and Gauss weight function can give more stable results than the cone weight function are shown in Fig. 7.

Moreover, with different discretization, the BMC results are compared with the results of the CVRKPM and RKPM [27], as presented in Fig. 8. The discrete size $h$ denotes the distance between two adjacent boundary discrete nodes. It can be noted that the BMC and CVRKPM yield better results than the RKPM with identical discretization. In addition, the presented method gives more precise numerical results than CVRKPM as the number of discrete nodes increases.

## 4.2 A simply supported triangular plate

In this example, Fig. 9 shows that an equilateral triangular plate is subjected to a uniform force with a simply-supported boundary condition. Also, the analytical solution can be

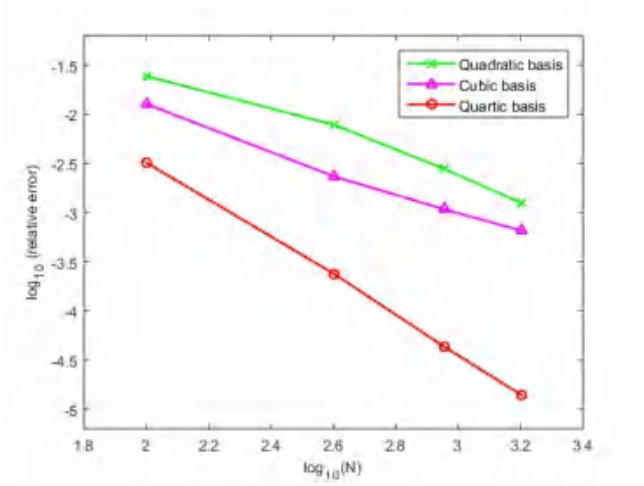


Figure 4: Relative error for the deflection norm with quadratic, cubic and quartic basis functions for a uniformly loaded square plate with all edges simply-supported.

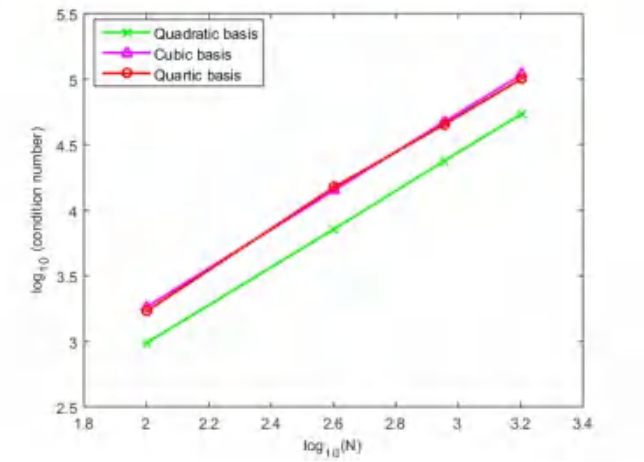


Figure 5: Condition number for the stiffness matrix with quadratic, cubic and quartic basis functions for a uniformly loaded square plate with all edges simply-supported.

written as

$$w = A\left\{x^3 - 3y^2x - a\left(x^2+y^2\right) + \frac{4}{27}a^3\right\}Z(x,y), \tag{4.3}$$

where $Z(x,y) = \frac{4}{9}a^2 - x^2 - y^2$, $A = \frac{q}{64aD}$, $q = 500\text{N/m}^2$, $a = \sqrt{3}/2\text{m}$, $E = 2.1\times10^{11}\text{Pa}$, plate thickness $h = 0.005\text{m}$, Poisson ratio $v = 0.25$.

The discretization of the BMC and FEM for the triangular plate problem is presented in Fig. 10. There are 265 triangular and 45 boundary elements employed in the FEM mesh

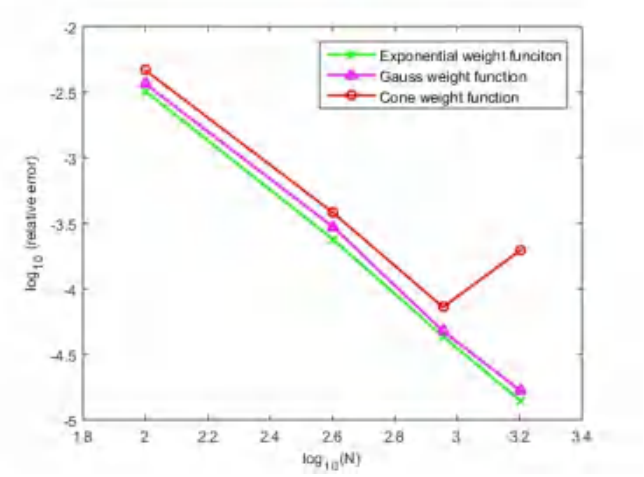


Figure 6: Relative error for the deflection norm with exponential, gauss and cone weight functions for a uniformly loaded square plate with all edges simply-supported.

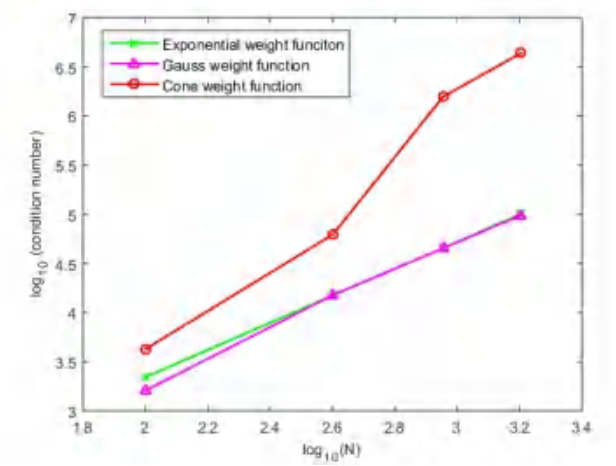


Figure 7: Condition number for the stiffness matrix with exponential, gauss and cone weight functions for a uniformly loaded square plate with all edges simply-supported.

pattern. And 21 boundary discrete nodes in each axis are adopted in the BMC discretization. The corresponding CPU times of the BMC and FEM are 0.2s and 2s, respectively. Fig. 11 shows the contours plot with the FEM and BMC for the triangular plate problem along $y=0$. The deflection relative errors of the BMC and FEM at the center point are 8.37e-5 and 8.31e-3, respectively. Fig. 12 shows the contour plot of the aforementioned FEM and BMC results. In general, it could be concluded that an excellent agreement between the BMC solutions and the exact solutions is achieved in this example.

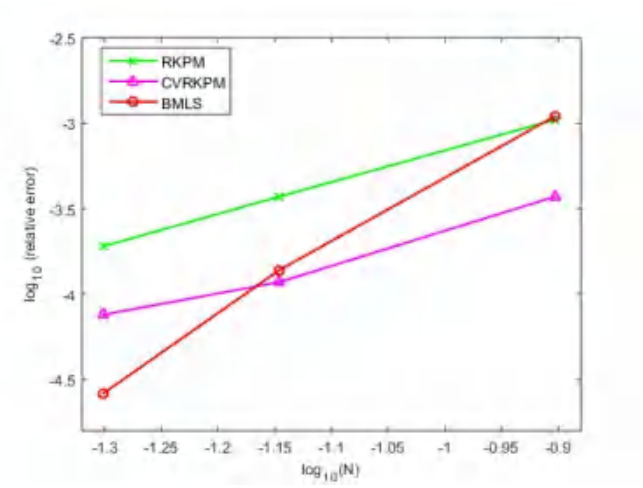


Figure 8: The relative errors for the RKPM, CVRKPM, and BMC.

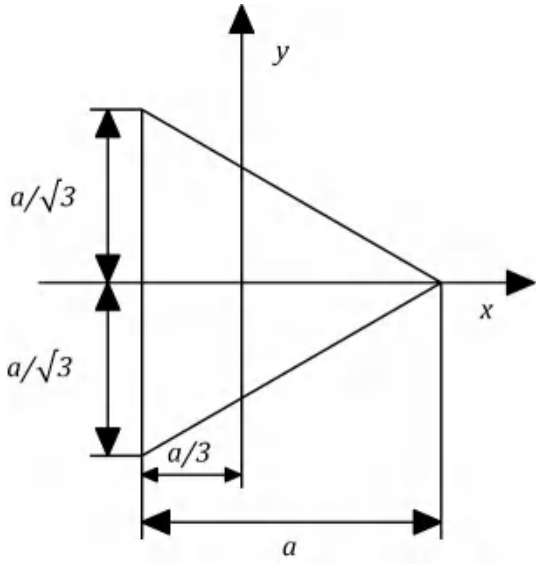


Figure 9: A triangular plate subjected to a uniformly distributed load with all edges simply-supported.

### 4.3 A clamped elliptical plate

In this example, Fig. 13 describes a clamped elliptical plate of axes $a$ and $b$ is subjected to a uniformly external force $q$. Also, the equation of elliptical edge shape is given as

$$\frac{x^2}{a^2}+\frac{y^2}{b^2}-1=0. \tag{4.4}$$

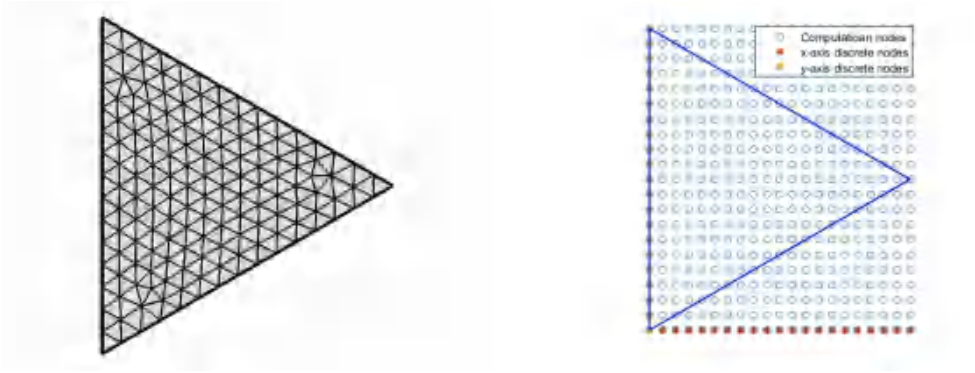


(a) FEM (b) BMC

Figure 10: The discretization for the triangular plate problem. (a) distribution of elements used in the FEM, (b) distribution of collocation nodes used in the BMC method.

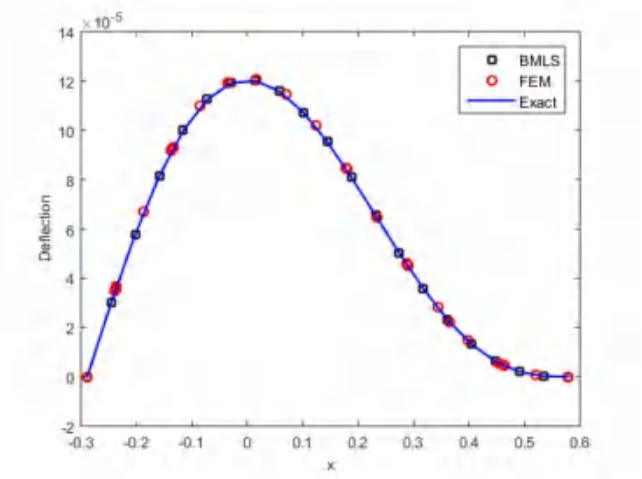


Figure 11: The deflection for the BMC, FEM, and exact results at $y=0$ for a triangular plate subjected to a uniformly distributed load with all edges simply-supported.

Meanwhile, the boundary conditions are given by

$$w=0, \quad \frac{\partial w}{\partial n}=0, \tag{4.5}$$

where $n$ is the normal vector for boundary $\Gamma$.

Also, the analytical solution to this problems is given as follows

$$w=\frac{q}{\left(\frac{24}{a^4}+\frac{24}{b^4}+\frac{16}{a^2b^2}\right)D}. \tag{4.6}$$

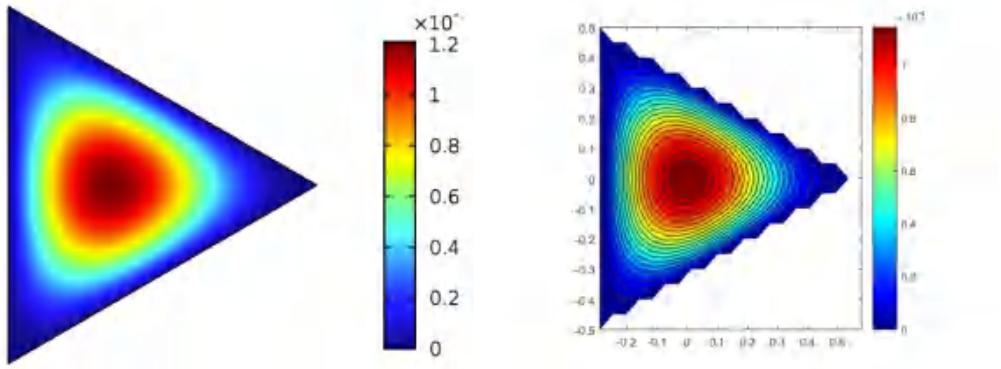


(a) FEM (b) BMC

Figure 12: Contours plot with the FEM and BMC for a triangular plate subjected to a uniformly distributed load with all edges simply-supported.

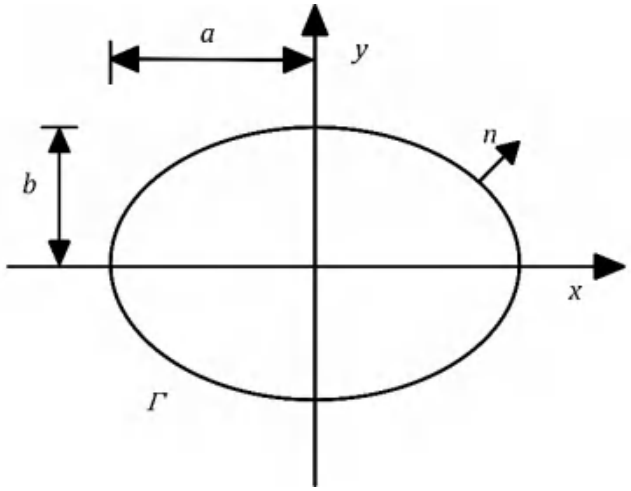


Figure 13: An elliptical plate subjected to a uniformly distributed load with all edges clamped.

In this regard, $a=1.5$m, $b=1$m, $q=500\text{N}/\text{m}^2$, $E=2.1\times10^{11}$Pa, $h=0.005$m, $v=0.25$. A non-uniform discretization type is adopted in the BMC as shown in Fig. 14(a), which includes 441 computational nodes. The corresponding mesh of FEM is presented in Fig. 14(b), which contains 400 quadrilateral grids, 80 boundary elements, and 441 vertices. The CPU times of the BMC and FEM are 0.05s and 3s, respectively. The deflection relative errors of the BMC and FEM at the central point are 8.51e−10, and 1.41e−4, respectively. Fig. 15 shows the deflection results from the BMC, FEM, and exact results at $\text{y}=0$ for the elliptical plate problem. In addition, Fig. 16 shows the contour plot of the FEM and BMC results for the elliptical plate. It can be concluded that the BMC approach yields approximation results with high precision.

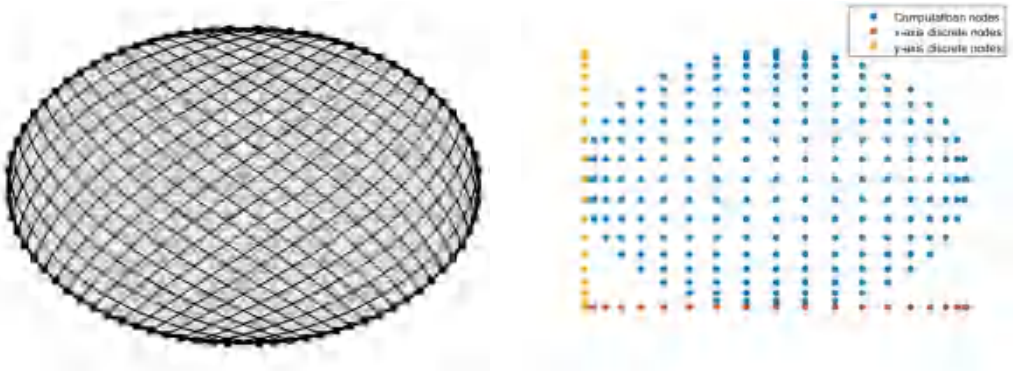

(a) FEM (b) BMC

Figure 14: The discretization for the elliptical plate problem. (a) distribution of elements used in the FEM, (b) distribution of collocation nodes used in the BMC method.

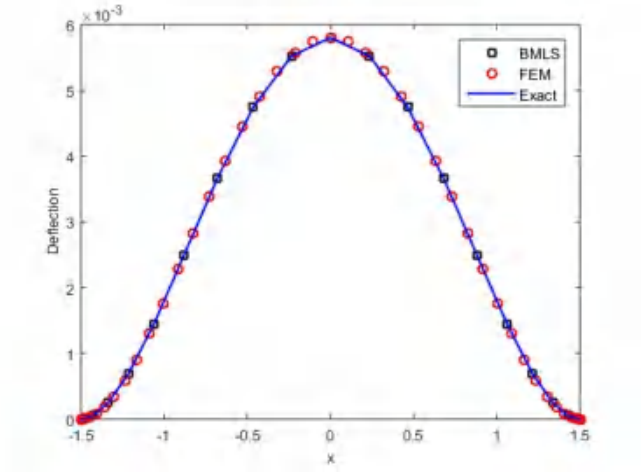


Figure 15: The deflection for the BMC, FEM, and exact results at $y=0$ for an elliptical plate subjected to a uniformly distributed load with all edges clamped.

## 4.4 An irregular shaped plate for computational efficiency

In the final example, Fig. 17 shows that a simply supported irregular-shaped plate is subjected to an external force $q$, which is applied to demonstrate the capability of the BMC for solving plate bending problems with irregular geometries.

In this regard, $a$=3m, $b$=4m, $c$=1.5m, $d$=1m, $q$=500N/m$^2$, $E$=2.1$\times$10$^{11}$Pa, $h$=0.005m, $v=0.25$.

Fig. 18 shows the discretization of the FEM and BMC for the irregular example. The meshes of FEM include 9900 quadrilateral and 496 boundary elements, and 10149 vertices. And 101 discrete nodes in each axis are adopted in the BMC discretization, which

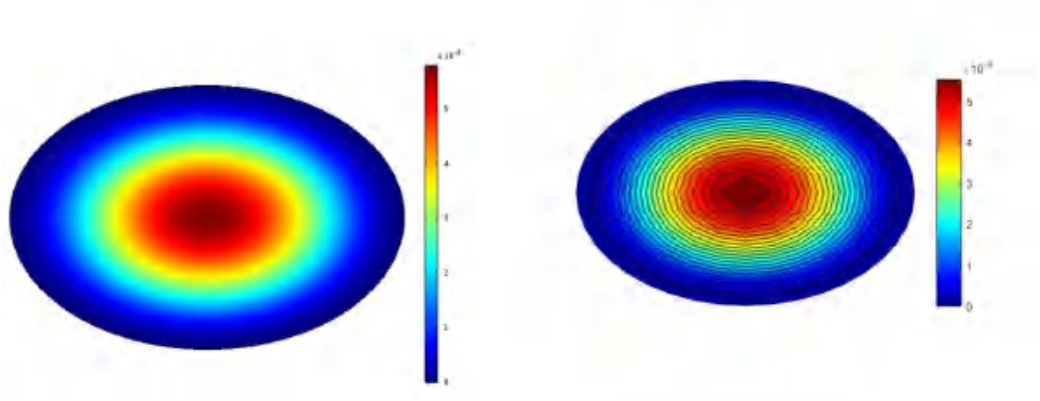

(a) FEM (b) BMC

Figure 16: The deflection results of the FEM and BMC for an elliptical plate subjected to a uniformly distributed load with all edges clamped. (a) the deflection result of the FEM, (b) the deflection result of the BMC method.

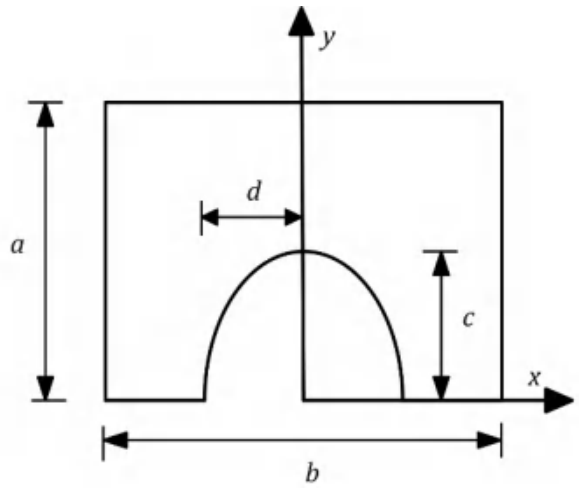


Figure 17: An irregular plate subjected to a uniformly distributed load with all edges simply-supported.

includes 10201 computational nodes. Fig. 19 shows the comparison of the deflection for these two methods along $y=2.01$. The maximum deflection for the BMC is 1.582e-2m, while the corresponding result of FEM is 1.585e-2m, and hence, the relative error between these two methods is 1.70e-3m. Fig. 20 shows the contour plot of the FEM and BMC results for the irregular plate. It can be seen that there is good agreement between the BMC and FEM results.

Moreover, Fig. 21 shows that the BMC approach takes less CPU time than the FEM with a similar node distribution. Hence, the proposed method possesses higher computational efficiency than the FEM in this numerical experiment.

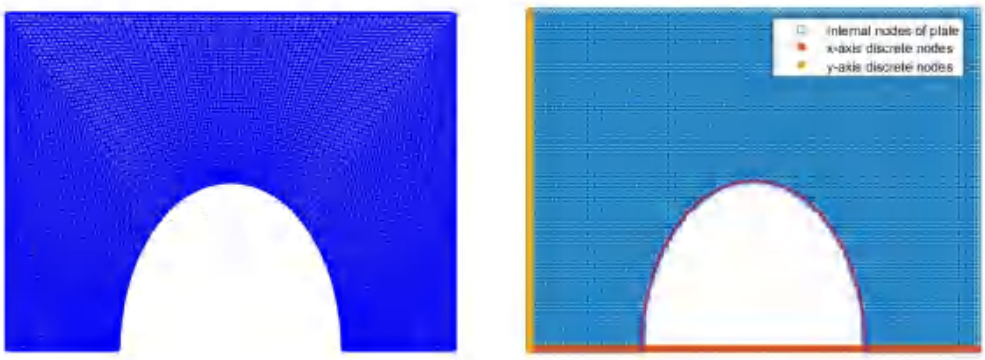


(a) FEM (b) BMC

Figure 18: The discretization for the irregular plate problem. (a) distribution of elements used in the FEM, (b) distribution of collocation nodes used in the BMC method.

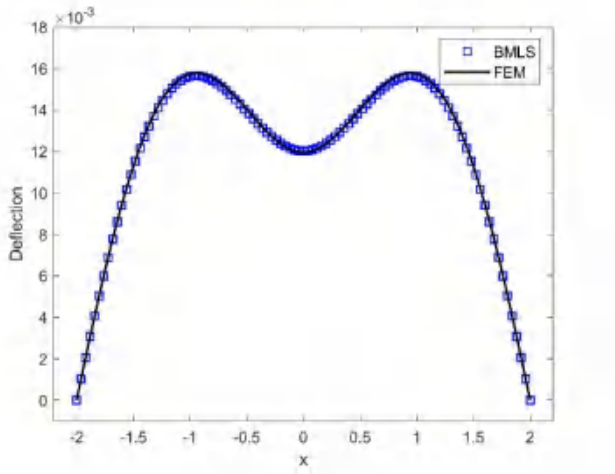


Figure 19: The deflection for the BMC and FEM exact results at $y=2.01$ for an elliptical plate subjected to a uniformly distributed load with all edges simply-supported.

## 5 Conclusions

In this work, the BMC method is proposed for approximating the deflection function of the thin plates under transverse loading conditions with different boundary conditions. The presented approach applies the 1D basis function and 1D weight function to solve the 2D plate bending problems. Hence, the 2D deflection function has been approximated via the Kronecker product operation with 1D moving least squares technique. Moreover, employing the virtual boundary method satisfies the boundary conditions for the BMC implementation. Notably, only boundary discrete nodes on the axis are contained within

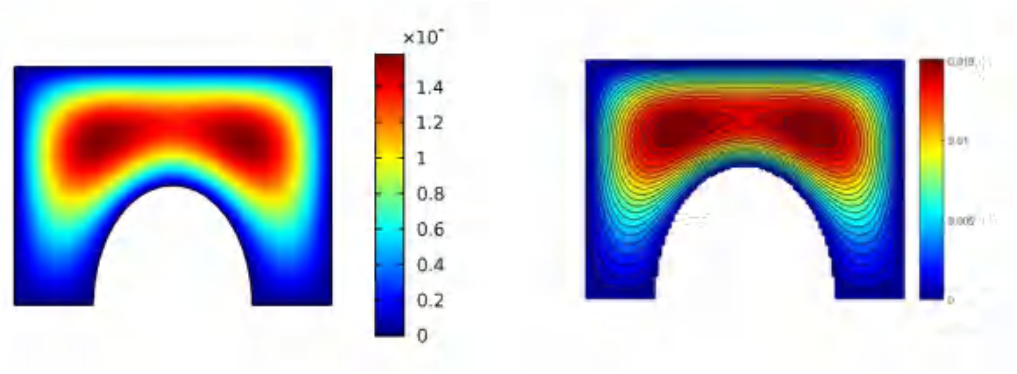


(a) FEM (b) BMC

Figure 20: Contours plot with the FEM and BMC for an irregular plate subjected to a uniformly distributed load with all edges simply-supported.

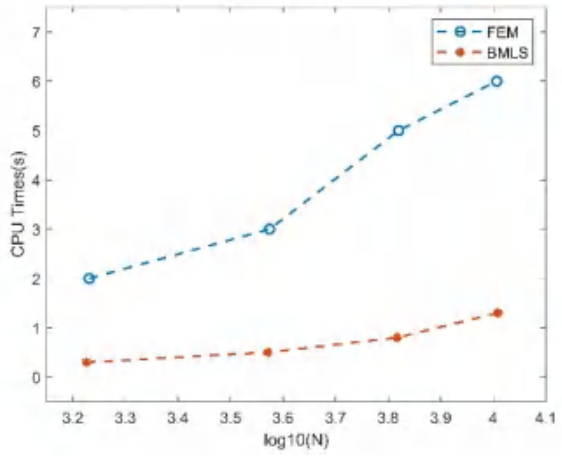


Figure 21: The CPU times of the BMC and FEM for an irregular plate subjected to a uniformly distributed load with all edges simply-supported.

the BMC pre-processing, and the tensor product nodes are generated automatically in the computational domain.

Convergence and stability analysis in the well-known benchmark shows that the proposed approach owns a strong convergence and stability while employing the quartic basis and the exponential weight function can provide more agreement with both the exact results and existing numerical solutions. Additionally, several numerical examples have been given to verify the BMC method is accurate and efficient for different shapes of thin plates and various boundary conditions. Meanwhile, highly accurate approximate solutions have been obtained employing a few discretized nodes on the axis within the BMC approach. Besides, for all these examples, a comparison of the BMC based deflec-

tion results with pertinent FEM data has been introduced for the accuracy and reliability evaluation. Furthermore, a comparison of the CPU times between the BMC and FEM shows the proposed method has a good computational efficiency for the bending problem of Kirchhoff plates.

## Acknowledgements

This work is supported by GuangDong Basic and Applied Basic Research Foundation (No. 2021A1515110807), the PhD Starting Foundation of Nanchang Hangkong University (No. EA202411285), the Program for Guangdong Introducing Innovative and Entrepreneurial Teams (No. 2019ZT08G315) and National Natural Science Foundation of China (No. U19A2098).

## References

[1] A. PIRROTTA, AND C. BUCHER, *Innovative straight formulation for plate in bending,* Comput. Struct., 180 (2017), pp. 117–124.
[2] J. KATSIKADELIS, Boundary Elements: Theory and Applications, UK: Elsevier Science Ltd., 2002.
[3] T. HROMADKA, The Complex Variable Boundary Element Method, Berlin, Heidelberg, New York, Tokyo: Springer-Verlag, 1984.
[4] G. BARONE, A. PIRROTTA AND R. SANTORO, *Comparison among three boundary element methods for torsion problems: CPM, CVBEM, LEM,* Eng. Anal. Boundary Elem., 35 (2011), pp. 895–907.
[5] G. BARONE AND A. PIRROTTA, *CVBEM for solving De Saint-Venant solid under shear forces,* Eng. Anal. Boundary Elem., 139(9) (2013), pp. 197–204.
[6] G. LIU, Mesh Free Methods, 1st ed. CRC Press, 2002.
[7] S. LI AND W. LIU, Meshfree Particle Methods, Berlin: Springer Verlag, 2004.
[8] Y. LIU, Y. HON AND K. LIEW, *A meshfree Hermite-type radial point interpolation method for Kirchhoff plate problems,* Int. J. Numer. Methods. Eng., 66 (2006), pp. 1153–1178.
[9] NEVINE A. MARKOUS, *Boundary mesh free method with distributed sources for Kirchhoff plate bending problems,* Appl. Math. Model., 94 (2021), pp. 139–151.
[10] V. LEITAO, *A meshless method for Kirchhoff plate bending problems,* Int. J. Numer. Methods Eng., 52 (2001), pp. 1107–1130.
[11] X. LONG, H. XIE, X. DENG, X. WEN, J. QU, R. QU, J. WANG AND F. LIU, *Geological and geochemical characteristics of the geothermal resources in Rucheng, China,* Lithospere-US, 5 (2021), 1357568.
[12] L. LUCY, *A numerical approach to the testing of the Assion hypothesis,* Astron. J., 82(12) (1997), pp. 1013–1024.
[13] B. NAYROLES, G. TOUZOT AND P. VILLON *Generalizing the finite element method: diffuse approximation and diffuse elements,* Comput. Mech., 10 (1992), pp. 307–318.
[14] T. BELYSCHKO, Y. LU, AND L. GU, *Element free Galerkin methods,* Int. J. Numer. Methods Eng., 37 (1994), pp. 229–256.

[15] W. Liu, S. Jun and Y. Zhang, *Reproducing kernel particle methods,* Int. J. Numer. Methods Fluids, 20(8) (1995), pp. 1081–1106.
[16] C. Duarte and J. Oder, *An h-p adaptive method using clouds,* Comput. Method Appl. M., 139(1-4) (1996), pp. 237–262.
[17] S. Atluri and T. Zhu, *A new meshless local Petrov–Galerkin (MLPG) approach in computational mechanics,* Comput. Mech., 22(2) (1998), pp. 117–127.
[18] E. Onate, F. Perazzo and J. Miquel, *A finite point method for elasticity problems,* Comput. Struct., 79(22-25) (2001), pp. 2151–2163.
[19] K. Lam, Q. Wang and H. Li, *A novel meshless approach-Local Kriging (LoKriging) method with two-dimensional structural analysis,* Comput. Mech., 33 (2004), pp. 235–244.
[20] Y. Gu, Q. Wang and K. Lam, *A meshless local Kriging method for large deformation analyses,* Comput. Methods Appl. M., 196 (2007), pp. 1673–1684.
[21] L. Chen and K. Liew, *A local Petrov–Galerkin approach with moving Kriging interpolation for solving transient heat conduction problems,* Comput. Mech., 47 (2011), pp. 455–467.
[22] K. Liew, J. Wang, M. Tan and S. Rajendran, *Nonlinear analysis of laminated composite plates using the mesh-free kp-Ritz method based on FSDT,* Int. J. Numer. Methods Eng., 193 (2004), pp. 4763–4779.
[23] K. Liew, Y. Cheng, and S. Kitipornchai, *Boundary elementfree method (BEFM) and its application to two-dimensional elasticity problems,* Int. J. Numer. Methods Eng., 65(8) (2006), pp. 1310–1332.
[24] Y. Cheng and M. Peng, *Boundary element-free method for elastodynamics,* Sci. China Ser. G., 48(6) (2005), pp. 641–657.
[25] Y. Cheng, K. Liew and S. Kitipornchai, *Reply to Comments on Boundary elementfree method (BEFM) and its application to two-dimensional elasticity problems,* Int. J. Numer. Methods Eng., 78 (2009), pp. 1258–1260.
[26] Z. Zhang, K. Liew and Y. Cheng, *Coupling of the improved element-free Galerkin and boundary element methods for two dimensional elasticity problems,* Eng. Anal. Boundary Elem., 32(2) (2008), pp. 100–107.
[27] L. Chen, Y. Cheng and H. Ma, *The complex variable reproducing kernel particle method for the analysis of Kirchhoff plates,* Comput. Mech., 55 (2015), pp. 591–602.
[28] S. Cheng, F. Wang, G. Wu and C. Zhang, *A semi-analytical and boundary-type meshless method with adjoint variable formulation for acoustic design sensitivity analysis,* Appl. Math. Lett., 131 (2022), 108086.
[29] F. Wang, Q. Zhao, Z. Chen and C. Fan, *Localized Chebyshev collocation method for solving elliptic partial differential equations in arbitrary 2D domains,* Appl. Math. Comput., 397 (2021), 125903.
[30] Z. Chen and F. Wang, *Localized method of fundamental solutions for acoustic analysis inside a car cavity with sound-absorbing material,* Adv. Appl. Math. Mech., 15 (2023), pp. 182–201.
[31] J. Kołodziej, and A. Zielinski, Boundary Collocation Techniques and Their Application in Engineering, WIT Press, 2009.
[32] P. Krysl and T. Belytschko, *Analysis of thin plates by elementfree Galerkin method,* Comput. Mech., 17 (1995), pp. 26–35.
[33] P. Krysl and T. Belytschko, *Analysis of thin shells by the element-free Galerkin method,* Int. J. Solid. Struct., 33 (1996), pp. 3057–3080.
[34] S. Sadamoto, S. Tanaka, K. Taniguchi, M. Ozdemir, T. Bui, C. Murakami, and D. Yanagihara, *Buckling analysis of stiffened plate structures by an improved meshfree flat shell formulation,* Thin-Walled Struct., 117 (2017), pp. 303–313.

[35] S. SADAMOTO, M. OZDEMIR, S. TANAKA, K. TANIGUCHI, T. YU, AND T. BUI, *An effective meshfree reproducing kernel method for buckling analysis of cylindrical shells with and without cutouts,*, Comput. Mech., 59 (2017), pp. 919–932.
[36] S. LONG AND S. ATLURI, *A meshless local Petrov–Galerkin method for solving the bending problem of a thin plate,* Comput. Model. Eng. Sci., 3(1) (2002), pp. 53–63.
[37] G. BATTAGLIA, A. DI MATTEO, G. MICALE AND A. PIRROTTA, *Arbitrarily shaped plates analysis via line Element-Less method (LEM),* Thin Wall Struct., 133 (2018), pp. 235–248.
[38] Z. HUANG, D. LEI, Z. HAN, H. XIE, AND J. ZHU, *Space–time collocation meshfree method formodeling 3D wave propagation problems,* Comput. Mech., (2023).
[39] Z. HUANG, D. LEI AND Y. WANG, *Modified moving least square collocation method for solving wave equations,* Adv. Appl. Math. Mech., 10 (2019), pp. 1–17.
[40] Z. HUANG, D. LEI, D. HUANG, J. LIN AND Z. HAN, *Boundary moving least square method for 2D elasticity problems,* Eng. Anal. Boundary Elem., 106 (2019), pp. 505–512.
[41] Z. HUANG, D. LEI, Z. HAN AND P. ZHANG, *Boundary moving least square method for numerical evaluation of two-dimensional elastic membrane and plate dynamics problems,* Eng. Anal. Boundary Elem., 108 (2019), pp. 41–48.
[42] Z. HUANG, D. LEI, Z. HAN AND J. LIN, *Boundary moving least square method for 3D elasticity problems,* Eng. Anal. Boundary Elem., 121 (2020), pp. 255–266.